phys. stat. sol. (a) **23**, 187 (1974)

Subject classification: 14.3.2 and 18.3; 13.5.4; 22.2.3; 22.8.2

Philips Forschungslaboratorium Hamburg GmbH

Magnetostatic Wave Drag on Electrons in a Hybrid Sample of YIG and InSb

By

B. SCHNEIDER

In a hybrid sample composed of a ferrimagnetic YIG plate and a semiconducting InSb plate, a magnetostatic spin wave propagating along the ferrimagnetic plate exercises a drag on the electrons in the semiconductor plate. The resulting magnon drag voltage has been investigated as a function of applied magnetic field strength (0 to 3.5 kOe), spin wave power (5 to 500 μW), sample temperature (4 to 300 K), and frequency (1 to 3 GHz). The experimental results above 30 K could be explained by a theoretical treatment. This is based on the assumption of a non-linearity in the field equations caused by the magnetic field dependence of the conductivity tensor for the semiconductor.

In einer hybriden Probe, die aus einer ferrimagnetischen YIG-Platte und einer halbleitenden InSb-Platte zusammengesetzt ist, führt eine magnetostatische Spinwelle, die sich längs der ferrimagnetischen Platte fortpflanzt, Elektronen in der angrenzenden Halbleiterplatte mit. Die resultierende Magnon-Mitführungsspannung wurde als Funktion der angelegten Magnetfeldstärke (0 bis 3,5 kOe), der Spinwellenleistung (5 bis 500 μW), der Probentemperatur (4 bis 300 K) und der Frequenz (1 bis 3 GHz) untersucht. Die experimentellen Ergebnisse oberhalb 30 K wurden durch eine theoretische Behandlung gedeutet. Diese ist auf die Annahme einer Nichtlinearität der Feldgleichungen gegründet, die auf der Magnetfeldabhängigkeit des Leitfähigkeitstensors des Halbleiters beruht.

1. Introduction

If a wave is propagating through a medium containing free charge carriers and if there is an interaction between the wave and the carriers, two effects may be observed:

1) the wave will be attenuated (or may be amplified if an appropriate drift motion is imposed on the carriers) [1],

2) a drag will be exerted by the wave on the charge carriers [2].

For ultrasound these effects (acousto-electric effects) were thoroughly investigated by many researchers after the pioneering work by Hutson et al. [1] on acoustic amplifiers and by Weinreich [2] on the acousto-electric drag voltage. We have performed similar experiments with magnetostatic spin waves. In a former paper, experimental evidence has been presented of a strong interaction between magnetostatic waves in a ferrimagnetic insulator and electrons in an adjacent semiconductor across the common interface of a hybrid sample [3]. Furthermore, we have shown that the attenuation of a magnetostatic wave in such a sample can be influenced by an electric drift current [4]. In this paper, we are reporting on the experimental and theoretical investigation of the drag voltage caused by magnetostatic spin waves, a new effect which had not been observed before. In the accepted terminology, the name of this effect should be "magnetostatic spin wave–electron-drag

voltage", but for short we call it just "magnon drag (m. d.) voltage". The interpretation of this new effect is based on the magnetic field dependence of the electric conductivity of the semiconductor. An approximate evaluation of the theory allows to explain the experimental results in the temperature range from 30 to 300 K.

2. Experiment, Apparatus, and Evaluation

2.1 Experimental arrangement

The experimental arrangement is shown in Fig. 1. The hybrid sample is composed of a thin ferrimagnetic plate of yttrium iron garnet (YIG) and a thin semiconducting plate of InSb with their mechanically polished faces pressed on each other. A magnetic bias field $\boldsymbol{H}^0$ (0 to 3.5 kOe) is applied parallel to the long edges (x_3-axis) of the sample. At one end of the ferrimagnetic plate, magnetostatic spin waves are excited by a microwave power P_0 through a thin wire antenna (left). The spin waves travel along the plate, and the transmitted output power P_{op} is received at the other end by a second thin wire antenna (right). The magnetic and electric fields of the wave fringe out of the ferrimagnetic plate into the semiconductor plate and cause an interaction with the charge carriers there. As the wave is propagating, a drag is exerted on the electrons and a dc voltage U_3 builds up at the ends of the semiconductor plate. This voltage is of the order of 1 to 1000 nV and has been measured as a function of bias magnetic field, spin wave power P_{spw} (5 to 500 μW), temperature T (4 to 300 K), and frequency (1 to 3 GHz).

2.2 Measurement of spin wave power and attenuation

In these experiments, a radio frequency power P_0 of about 5 mW is supplied to the input antenna, but only a very small fraction P_{spwo} of this is converted into spin wave power. This fraction has been determined by measuring the deficit of the power reflected from the input antenna. For these measurements a reference point is used at a high magnetic bias field $\boldsymbol{H}^{\mathrm{r}}$, where no spin waves are generated, due to a cut-off in the excitation mechanism. The accuracy of this measurement could be considerably improved by using a compensation method in which the outputs of two powermeters of the same type were con-

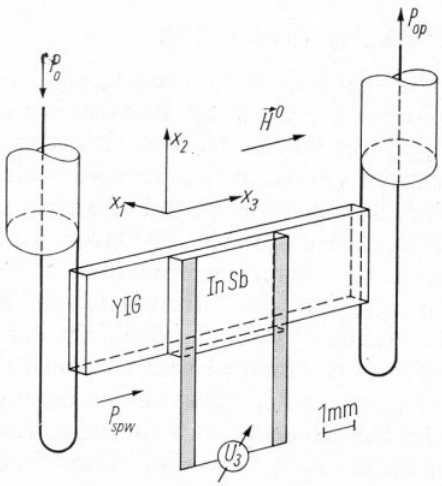

Fig. 1. Schematic view of the sample arrangement for the measurement of the magnon drag voltage

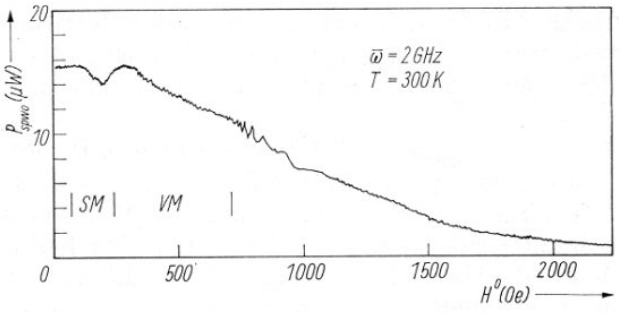

Fig. 2. The spin wave power P_{spwo} excited at the front end of the hybrid sample at constant excitation power P_0 versus applied magnetic field strength H^0. The reference point is at $H^{\mathrm{r}} = 3.5$ kOe. (SM surface mode range, VM volume mode range)

nected in series opposite. The first one of these powermeters measures the power reflected from the input antenna, the other one is driven by a fraction of the input power, adjusted such as to compensate the reading of the first powermeter at the reference magnetic field $\boldsymbol{H}^{\mathrm{r}}$. The differential reading is corrected for the attenuations and the reflections of the wave on the transmission line and in the different components passed, and then yields the spin-wave power excited in the sample. In Fig. 2 the magnetic field dependence of the excited spin-wave power P_{spwo} is presented. It is a rather smooth function of magnetic field, and its maximum at low magnetic field strength is 10 to 30 dB lower than the input power. At known input power P_0, this measurement also yields the coupling factor of the input antenna. Assuming reciprocity, the coupling factor of the output antenna may be determined in the same way. It should be noted, however, that the reciprocity theorem [6] used, does not apply strictly in this case and hence this assumption represents a crude approximation.

The attenuation of the spin wave in the sample can then be determined rather easily from the ratio of the spin-wave power P_{spwo} excited at the input end of the sample over the spin-wave power P_{tr} transmitted to the output end, detected by means of a calibrated superheterodyne receiver.

A curve representative of the magnetic field dependence of the output power P_{op} is given in Fig. 3a. The spectrum of magnetostatic modes through the YIG plate is modified by the presence of the InSb plate. The waves are strongly

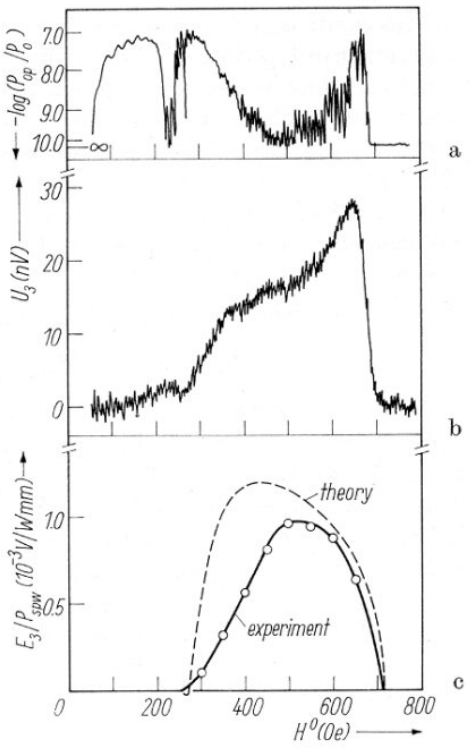

Fig. 3. a) The spin wave transmission given as transmitted output power P_{op} over excitation power P_0 on a logarithmic scale versus applied magnetic field strength H^0 for $T = 300$ K and $\bar{\omega} = 2$ GHz. b) The magnon drag voltage U_3 versus applied magnetic field strength H^0 for $T = 300$ K and $\bar{\omega} = 2$ GHz. c) The magnon drag field strength E_3 over local spin wave power P_{spw} versus magnetic field strength H^0. (Experimental curve derived from 4b)

damped by their interaction with the electrons in the semiconductor [3]. The basic feature, however, remains: distinct ranges of magnetostatic surface modes ($H^0 = 50$ to 230 Oe in Fig. 3a) and volume modes ($H^0 = 230$ to 700 Oe).

2.3 Measurement of the drag voltage

In our set-up, the drag voltage U_3 is typically of the order of nV. In order to facilitate its measurement and to eliminate spurious thermovoltages, a lock-in technique has been used. The r.f. power has been chopped at a frequency of about 975 Hz and the drag voltage detected by a lock-in amplifier. By the input of chopped r.f. power, there may also be generated a pulsating thermovoltage. This thermovoltage, however, is shifted by $\pi/2$ in phase and can thus be eliminated by careful adjustment of the phase-sensitive detector.

Another source of error could be a non-ohmic behavior of contacts of the leads to the InSb plate. If the contact resistance depends on the current, this may result in a rectification and may add a dc voltage to the magnon drag voltage. By using In-Te solder [5] we were able to keep this effect small as has been checked by direct measurements. Only below 30 K, the non-linearity of the contacts increased considerably and might have caused non-negligible errors.

A curve representative of the measured drag voltage U_3 versus magnetic field is presented in Fig. 3b. At low magnetic fields, in the range of surface modes, the drag voltage is rather small, but increases in the range of volume modes with increasing magnetic field and then, at the mode cut-off, sharply drops to zero. We are going to consider only the larger effects in the volume mode range.

2.4 Evaluation of the experimental results

The results of these experiments are total voltages U_3 along the sample for a given input power P_0. For comparison with the theoretical calculations, one wants to derive from the voltage a local field strength E_3 per unit local spin-wave power P_{spw}. In this evaluation, the attenuation of the spin wave along the sample has to be taken into account. This will be possible, if one assumes that the dc field strength generated is proportional to the local spin-wave power, which may be concluded from the experimental fact that the total voltage U_3 is proportional to the spin-wave power P_{spwo} (see below). The results of this calculation, E_3/P_{spw} derived from the magnon drag voltage U_3, are given in Fig. 3c, 7, and 8.

3. Experimental Results

As shown in Fig. 3c ($T = 300$ K, $\overline{\omega} = 2$ GHz), E_3/P_{spw} depends strongly on the applied magnetic field strength H^0. This field dependence is very similar for all temperatures and frequencies.

If the voltage measured is really caused by a drag effect, it should be reversed if the direction of transmission is reversed. In Fig. 4 the magnetic field dependence of the drag voltage for a propagation vector $+\boldsymbol{k}$ and a magnetic field $+\boldsymbol{H}^0$ is compared with the corresponding curve where the direction of transmission is reversed ($-\boldsymbol{k}$, $+\boldsymbol{H}^0$). The sign of the voltage is reversed, but the amplitude has changed, too. The reasons are that (i) the coupling constant of the second antenna at the other end of the sample is somewhat different and (ii) the voltage generated depends also on the direction of the magnetic field. The second

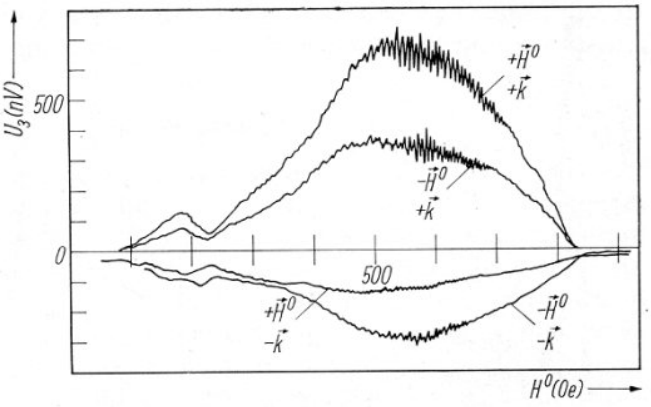

Fig. 4. Magnon drag voltage U_3 for different directions of the applied magnetic field strength $\boldsymbol{H}^0$ and of the spin wave vector $\boldsymbol{k}$ versus the magnitude of the applied magnetic field H^0

statement is demonstrated by comparing the curves, where the propagation direction has been retained but the magnetic field has been reversed, i.e. $(\boldsymbol{k}, +\boldsymbol{H}^0)$ and $(\boldsymbol{k}, -\boldsymbol{H}^0)$. This effect can be explained by the theory given below. In our experiments, the directions of $\boldsymbol{k}$ and $\boldsymbol{H}^0$ have always been chosen such as to make the resulting voltage a maximum.

The sign of the drag voltage is such as one will expect, if the electrons are dragged along by the phase propagation of the wave. As the magnetostatic volume modes are backward waves, this is opposite to the direction of energy transport.

Very important for the interpretation of these effects is the power dependence of the magnon drag voltage. In Fig. 5, the maximum voltage generated $U_3^{\max}$ is plotted versus spin-wave power P_{spwo} on a bilogarithmic scale for a fixed frequency of 2 GHz and a temperature of 70 K. At lower powers, the measured points lie quite well on a straight line of slope 1, i.e. the voltage is proportional to the power; in other words, the magnon drag voltage is a quadratic, second-order effect. At higher powers, the slope becomes smaller than 1, probably caused by the instability of the spin waves in the YIG plate.

In order to give a survey of its temperature and frequency dependence, the maximum magnon drag voltage per unit spin wave power $U_3^{\max}/P_{\text{spwo}}$ has been plotted in Fig. 6 versus temperature for various fixed frequencies between 1.2 and 2.88 GHz.

For the comparison of the experimental results with the theoretical calculations, two series of measurements have been performed very carefully, and all the corrections have been applied:

1. the temperature dependence of the magnon drag field strength E_3 at a constant frequency of $\overline{\omega} = 2.63$ GHz and an appropriately chosen (see below) magnetic field strength $\boldsymbol{H}^{\text{a}}$.

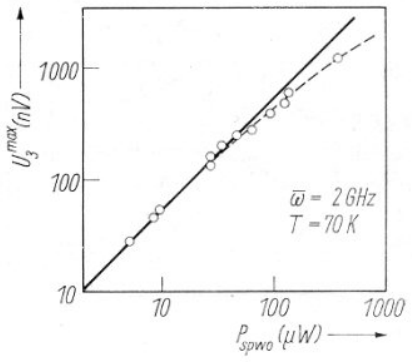

Fig. 5. The maximum magnon drag voltage $U_3^{\max}$ versus input spin wave power P_{spwo}

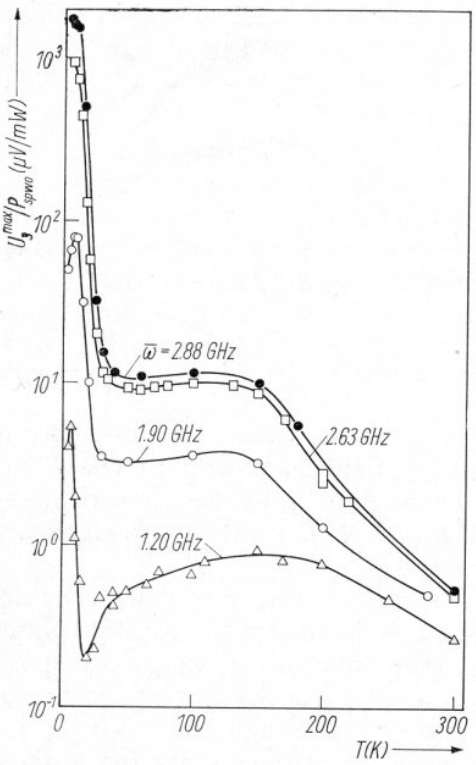

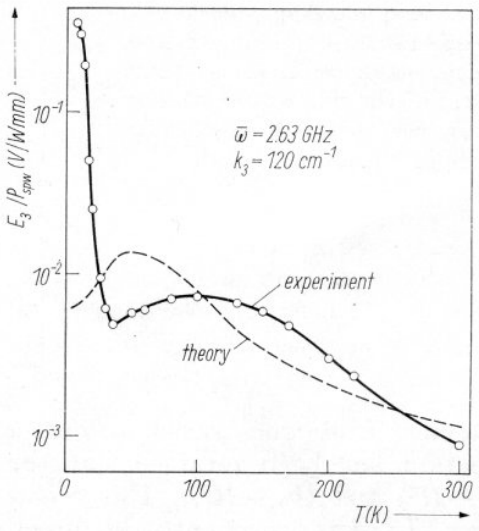

Fig. 7. The magnon drag field strength E_3 over local spin wave power P_{spw} for constant frequency $\bar{\omega} = 2.63$ GHz and constant spin wave vector component $k_3 = 120\ \mathrm{cm}^{-1}$ as a function of sample temperature T

Fig. 6. The maximum magnon drag voltage $U_3^{\max}$ over input spin wave power P_{spwo} versus sample temperature T for various frequencies $\bar{\omega}$ between 1.20 and 2.88 GHz

2. the frequency dependence of the m.d. field strength at a constant temperature $T = 70$ K and the magnetic field strength $\boldsymbol{H}^{\mathrm{a}}$.

The magnetic field H^{a} is chosen such that the wave vectors of the spin waves will be

$$k_3 = \frac{2\pi}{\lambda} = 120\ \mathrm{cm}^{-1}\,. \tag{1}$$

For all the frequencies and temperatures, H^{a} will lie near the maximum of the drag voltage and near the centre of the volume mode range.

The temperature dependence of the magnon drag field strength is given in Fig. 7. It roughly follows the voltage curve $U_3^{\max}(T)$ shown in Fig. 6. The frequency dependence of the magnon drag field strength is given in Fig. 8. The

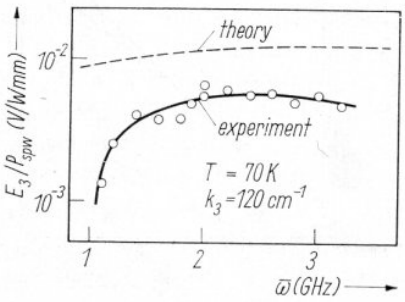

Fig. 8. The magnon drag field strength E_3 over local spin wave power P_{spw} for constant temperature $T = 70$ K and constant spin wave vector component $k_3 = 120\ \mathrm{cm}^{-1}$ as a function of frequency $\bar{\omega}$

variation is rather small. At low frequencies, there is a drop caused by the increasing attenuation of the spin wave by YIG, especially at the unsaturated ends of the crystal plate.

4. Theoretical Treatment

As in these experiments there is $\hbar\omega \ll k_B T$ and $\omega\tau \ll 1$ (with $\hbar$ Planck's constant, k_B Boltzmann's constant, and τ electron collision time), a phenomenological treatment is appropriate. The system is described by a set of non-linear electromagnetic field equations, by the equations of motion of the spins in the ferro(i)magnet and of the electrons in the semiconductor, and, further, by the boundary conditions between the three regions, ferromagnet, semiconductor, and vacuum. In a first approximation step, the electric and magnetic r.f. fields have been found from the linearized system of differential equations. In a second approximation step, the non-linearity has been introduced which yields the dc magnon drag current leading to the built-up of the magnon drag voltage.

4.1 First approximation step

Here a rather crude theoretical model is used. The electromagnetic field in the ferro(i)magnetic plate is calculated using the theory of Damon and Eshbach [7] without taking into account the semiconductor plate. The scalar potential for the magnetic field in the interior of the ferro(i)magnetic plate is taken to be of the wave form:

$$\psi^{\text{int}} = (A \cos k_1 x_1 \sin k_2 x_2 + B \sin k_1 x_1 \cos k_2 x_2) \exp\left(i(k_3 x_3 + \omega t)\right) \tag{2}$$

which describes the mode excited strongest by the present configuration of the antenna. For a ferro(i)magnetic plate in vacuum, the ratio of the coefficients A and B is defined by the boundary conditions yielding

$$\frac{A}{B} = \frac{-\chi_{12} k_2 \sin k_1 u}{(1 + \chi_{11}) k_1 \sin k_1 u - k^s \cos k_1 u}. \tag{3}$$

Here χ_{ij} is the r.f. susceptibility tensor, $2u$ the thickness of the plate, $k^s = \sqrt{k_1^2 + k_2^2}$. This expression will be adopted also for the hybrid system.

To approximate the boundary condition at the long edges of the sample, the propagation vector in x_2 direction is assumed to be $k_2 = \pi/b$, where b is the width of the sample. Then k_1 and k_3 are found from the dispersion equation of the fundamental mode of magnetostatic waves in a plate, as given in [8], by progressive approximation.

The electric field of the spin wave is found from its magnetic field by application of the second Maxwell equation.

For the fields in the semiconductor plate the following expression is used:

$$f_i = (f_i^c \cos k_2 x_2 + f_i^s \sin k_2 x_2) \exp\left(-\operatorname{Re}(k_1^{\text{ext}})\, x_1\right) \exp\left(i(k_3 x_3 + \omega t)\right), \tag{4}$$

where f_i stands for the electric and magnetic r.f. fields e_i and h_i. The wave vector component k_1^{ext} is found from the dispersion equation of a quasistatic wave in a conductor, where the influence of the applied magnetic field is neglected:

$$(k_1^{\text{ext}})^2 + k_2^2 + k_3^2 + i\mu^0 \omega\sigma = 0, \tag{5}$$

where μ^0 is the permeability of the semiconductor and σ the conductivity of the semiconductor. As, in the dispersion equation of the spin wave, damping has

been neglected, k_2 and k_3 are real. The wave vector component k_1^{ext} as derived from equation (5) is complex, but for the sake of simplicity we approximate the oscillating decay by an exponential, i.e. the imaginary part of k_1^{ext} is neglected and only the real part $\text{Re}(k_1^{\text{ext}})$ is introduced into equation (4). The coefficients f_i^{c} and f_i^{s} are found from the boundary condition for e_i and h_i at the interface between the ferromagnet and the semiconductor.

From these fields found in the first approximation step, the transport of energy through the system, needed for the calculation of E_3/P_{spw}, is calculated by integrating the Poynting vector over the cross section of the sample and the exterior of the sample.

4.2 Second approximation step

In second approximation the non-linearity is introduced into the calculation. For the acousto-electric effect this is done by introducing the modulation of charge carrier density by the electric field. If one does the same for this system, the calculated magnon drag voltage will be several orders of magnitude smaller than the experimental values. In the case of magnon drag the essential non-linearity is caused by the dependence of the conductivity tensor σ_{ij} in the semiconductor on the magnetic field, the more so, as for magnetostatic waves, h_i is comparatively large.

$$\sigma_{ij} = \sigma_{ij}(H_k) \,, \tag{6}$$

$$H_k = H_k^0 + h_k \,, \tag{7}$$

where H_k^0 is the applied magnetic field and h_k the h.f. magnetic field. σ_{ij} can be expanded into powers of h_k

$$\sigma_{ij}(H_k) = \sigma_{ij}(H_k^0) + \left[\frac{\partial}{\partial H_k}\sigma_{ij}(H_k)\right]_0 h_k + \cdots \,. \tag{8}$$

The current density in second approximation then is

$$j_i^{(2)} = \sigma_{ij}(H_k^0)\, e_j^{(1)} + \left[\frac{\partial}{\partial H_k}\sigma_{ij}(H_k)\right]_0 \cdot e_j^{(1)} h_k^{(1)} + \cdots \,, \tag{9}$$

where $e_j^{(1)}$ and $h_k^{(1)}$ are the field strengths in first approximation. The second-order term contains a part of frequency $2\overline{\omega}$ and a dc part which represents the magnon drag current

$$j_i^{(2)\|} = \left[\frac{\partial}{\partial H_k}\sigma_{ij}(H_k)\right]_0 \cdot \frac{1}{2}\,\text{Re}\,(e_j^{(1)*} \cdot h_k^{(1)}) \,. \tag{10}$$

Here the fields $e_j^{(1)}$ and $h_k^{(1)}$ have been used in complex notation, the star signifying the complex conjugate.

From the resistivity tensor

$$\varrho_{ij} = \varrho^0(\delta_{ij} - \varepsilon_{ijk}\mu\mu^0 H_k) \tag{11}$$

with ϱ^0 scalar resistivity at zero magnetic field, μ mobility of the charge carriers, and ε_{ijk} antisymmetric unit tensor of the third rank, one finds the conductivity tensor by inversion, and the second order dc current density for our

configuration

$$j_3^{(2)\parallel} = \frac{\mu\mu^0\sigma^0}{1+(\mu\mu^0 H_3^0)^2}\left[\frac{1}{2}\,\mathrm{Re}\,(h_1^{(1)}e_2^{(1)*} - h_2^{(1)}e_1^{(1)*}) + \right.$$
$$\left. + \frac{1}{2}\,\mu\mu^0 H_3^0 \cdot \frac{1}{2}\,\mathrm{Re}\,(h_1^{(1)}e_1^{(1)*} + h_2^{(1)}e_2^{(1)*})\right] \qquad (12)$$

with $\sigma^0 = 1/\varrho^0$ and μ independent of H_3^0.

The current density $j_3^{(2)\parallel}$ is composed of two parts: the first part is an even function of the applied magnetic field, but an odd function of the vector product $\boldsymbol{e}_i \times \boldsymbol{h}_i$, the Poynting vector, and hence will reverse when the propagation direction is reversed. The second part is an odd function of the applied magnetic field, but an even function of the propagation vector of the wave. This is in qualitative agreement with the results shown in Fig. 4. In our numerical calculation the second part of (12) vanishes. This is connected to the fact that the coefficients f_i^c and f_i^s are purely real or imaginary in our approximation. In a more sophisticated approximation this will not be the case. An estimate shows that the second part will be of about the same magnitude as or rather smaller than the first part. Therefore, an improved calculation including the second part will yield results not much different.

The total current I_3 is found by integration over the cross section of the semiconductor plate. In the case of a voltage measurement, the drag current I_3 is compensated by a return current $-I_3$. The magnon drag field strength then is

$$E_3 = \frac{I_3}{\sigma^0 db}, \qquad (13)$$

where d is the thickness and b the width of the semiconductor plate. For the numerical evaluation σ^0 and μ have been derived from separate conductivity and Hall-effect measurements and E_3/P_{spw} has been calculated. The results of the calculation are plotted in Figs. 3c, 7, and 8 as dashed lines.

5. Discussion

The experimental and the theoretical curves of the magnetic field dependence of the magnon drag field strength in Fig. 3c show quite good qualitative agreement. Both curves have their maximum near the centre of the magnetostatic volume mode range and drop to zero at both ends.

The agreement between theoretical and experimental curves for the temperature dependence of the magnon drag field strength (Fig. 7) depends on the temperature range. At the higher temperatures from 80 to 300 K the agreement is quite good, the curves intersect twice. Between 35 and 80 K the deviation between the experimental and the theoretical curves becomes larger than a factor of two, but even down to 30 K one may claim qualitative agreement, as the trends of both curves are much the same. Below 30 K, however, the sharp increase of the experimental curve is not reproduced by the calculated curve.

For the frequency dependence of the magnon drag field strength, the theoretical calculations yield only a slight increase between 1 and 3 GHz (Fig. 8). Aside from a sharp drop at frequencies below 1.5 GHz, which is caused by high

spin-wave losses not included in the theoretical calculations, the course of the experimental curve is similar to that of the calculated curve. The whole curve, however, is shifted towards smaller values, as one might expect from the temperature dependence curve in Fig. 7.

On the whole, one can say that a fair degree of qualitative agreement between experiment and theory has been attained. This supports the main assumption of the theoretical treatment, that the non-linearity is brought into the system by the magnetic field dependence of the conductivity tensor. The deviations between theory and experimental are supposed to be due to a rather poor approximation for the first-order field parameters, which could be considerably improved at a rather high mathematical expense.

So far unclear are the experimental effects below 30 K, which are not described by this theory. There is some experimental indication, that in this range we are not dealing with bulk effects, but with magnetic field dependent contact effects. Further experiments are necessary for a clarification.

After these investigations, one may be encouraged to base calculations of the spin-wave amplification by drifted electrons on the assumptions used here. Perhaps, it will be possible to resolve the tremendous discrepancies [4, 9] encountered so far, and improve the understanding of these effects.

Further, it might be very interesting to perform similar experiments with ferromagnetic semiconductors. These experiments could give information on the interaction between the spin waves and the free charge carriers in these materials.

Acknowledgements

The author would like to thank V. Doormann for his valuable technical assistance with the experiments and the composition of computer programs. He is also pleased to thank W. Tolksdorf for supplying the YIG crystals [10] and K. Walther, E. Krätzig, and Profressor D. Polder for their helpful discussions.

References

[1] A. R. HUTSON, J. H. MCFEE, and D. L. WHITE, Phys. Rev. Letters **7**, 237 (1961).
[2] G. WEINREICH, T. M. SANDERS, JR., and H. G. WHITE, Phys. Rev. **114**, 33 (1959).
[3] B. SCHNEIDER, Appl. Phys. Letters **13**, 405 (1968).
[4] B. SCHNEIDER and H. J. SCHMITT, Nachrichtentech. Fachber. **35**, 633 (1968).
[5] E. V. GEORGE and G. BEKEFI, Appl. Phys. Letters **15**, 33 (1969).
[6] S. SILVER, Microwave Antenna Theory and Design, McGraw-Hill Book Company, Inc., New York, Toronto, London 1949.
[7] R. W. DAMON and J. R. ESHBACH, J. Phys. Chem. Solids **19**, 308 (1961).
[8] B. SCHNEIDER, phys. stat. sol. (b) **51**, 325 (1972).
[9] B. B. ROBINSON, B. VURAL, and J. P. PAREKH, IEEE Trans. Electron Devices **ED-17**, 224 (1970).
[10] W. TOLKSDORF, J. Crystal. Growth **3/4**, 463 (1968).
W. TOLKSDORF and F. WELZ, J. Crystal Growth **13/14**, 566 (1972).

(Received February 26, 1974)

Experimental setup in the Philips Forschungslaboratorium Hamburg in 1973
with Labor Assistant Volker Doormann

B. Hill, B. Schneider and Volker Doormann in 1973 (from left to right)